



Contents lists available at ScienceDirect

Spectrochimica Acta Part A: Molecular and Biomolecular Spectroscopy

journal homepage: www.elsevier.com/locate/saa

Development of a two-line DLAS sensor for liquid film measurement

Huinan Yang^a, Yufeng Guo^a, Chuanliang Li^b, Jin Tao^c, Yuexing Zhang^a, Weiwei Wu^a, Mingxu Su^{a,*}

^a School of Energy and Power Engineering, University of Shanghai for Science and Technology, No. 516, Jungong Road, Yangpu District, Shanghai, China

^b Taiyuan University of Science and Technology, No. 66, Waliu Road, Wanbailin District, Taiyuan City, Shanxi Province 030000, China

^c State Key Laboratory of Applied Optics, Changchun Institute of Optics, Fine Mechanics and Physics, Chinese Academy of Sciences, Changchun, Jilin 130033, China

ARTICLE INFO

Article history:

Received 3 June 2019

Received in revised form 23 July 2019

Accepted 23 July 2019

Available online 24 July 2019

Keywords:

Measurement

Diode laser absorption spectroscopy

Liquid film

Thickness

Temperature

ABSTRACT

The simultaneous measurements of multiple parameters (film thickness, temperature, etc.) of the liquid films are crucial for the design and optimization of relevant industrial processes. Here, a sensor based on diode-laser absorption spectroscopy (DLAS) was developed to simultaneously measure liquid water film thicknesses and temperatures by combining two diode lasers at different wavenumber positions, 6718.2 cm^{-1} and 7040.8 cm^{-1} . Serious beam steering effects can be avoided by adding an integrating sphere to improve the performance of the sensor for the investigations of dynamic films. The measurement accuracies of this sensor were firstly validated by a calibration tool with known film thicknesses and temperatures. It revealed that the averaged deviations between the measured film thicknesses/temperatures and the corresponding known parameters were 4.58% and 1.34%, respectively. The sensor was then employed to study liquid film evaporation processes on a horizontal quartz glass plate. The imaging method and the thermocouple were simultaneously employed to obtain the film thicknesses and temperatures to compare with the DLAS results. It showed that the average evaporation rates of the liquid films were $0.34/0.41/0.57\text{ }\mu\text{m/s}$ at different temperatures (340/360/390 K) of the heat gun outlet, respectively, and the evaporation rates increased with the increasing film temperatures. The whole evaporation process can be tracked with the sensor. Furthermore, the sensor was applied to simultaneously determine the variations of liquid film thicknesses and temperatures in a flow channel. It was found that the film temperatures remained almost constant during passage of low-amplitude surface waves at the film temperatures 308/315/323 K.

© 2019 Elsevier B.V. All rights reserved.

1. Introduction

The phenomena of liquid film formations, evaporations and flow exist in the industrial processes widely, such as thermal engineering, air conditioning and refrigeration, aerospace, petrochemical industry and other related fields. For instance, the formations and evaporations of falling films in the vertical tube evaporator [1], the formations of liquid films on the surface of the effervescent atomizer [2], the flow of liquid films on the rotating disk in spin coating process [3], the flow and cooling of falling films in a cooling tower [4], and the formations of liquid films of the urea-water solutions on the exhaust gas pipe in the selective catalytic reduction (SCR) system of the automobile exhaust denitrification [5]. The simultaneous measurements of multiple parameters (film thickness, temperature, etc.) of the liquid films are crucial for the design and optimization of relevant industrial processes.

Conventional temperature measurement techniques, such as thermocouple, are simple and inexpensive. But it is intrusive and not

suitable for ultra-thin liquid film measurements. The measurement methods for liquid film thicknesses are generally divided into two categories: the contact methods and non-contact methods. The measurement accuracies and measurement ranges of contact methods such as the capacitance method and conductance method, are influenced by the conductivities of liquid films, the waveforms of liquid film surfaces, and structure parameters of probes [6,7]. The non-contact measurement methods include the imaging techniques and optical techniques, etc. For the imaging techniques, the imaging method can obtain the liquid film thicknesses in real time with a high-resolution camera to photograph liquid films and the substrates. For example, Yan et al. [8] employed a CCD (Charge Coupled Device) camera to obtain the images of a free-falling liquid-film flow at different Reynolds numbers and then processed on a computer. Charogiannis et al. [9] combined the planer laser-induced fluorescence (PLIF) with particle tracking velocimetry (PTV) and infrared (IR) thermography for the measurement of the film-height, 2-D velocity, etc. Greszik et al. [10] combined the laser-induced fluorescence (LIF) and spontaneous Raman scattering for imaging water film thicknesses. Cherdantsev et al. [11] used the brightness-based laser-

* Corresponding author.

E-mail address: sumx@usst.edu.cn (M. Su).

induced fluorescence (BBLIF) technique to obtain three-dimensional high-speed dynamic measurements of liquid film, simultaneously with studying the elements of the dispersed phase. Hidrovo et al. [12] utilizes the emission-reabsorption laser-induced fluorescence (ERLIF) to accurately measure film thickness. The optical techniques are mainly based on the total reflection of light and laser spectroscopy, with the advantages of non-invasion, high sensitivity, and high accuracy, etc. For the method based on reflection, Leng et al. [13] determined liquid film thicknesses using a laser focus displacement meter with outstanding spatial resolution. For the method based on laser spectroscopy, Clark [14] developed the light absorption imaging technique (LAIT) for film thickness measurements to provide unparallel spatial information on the interfacial structure of falling liquid films. Porter et al. [15] developed a novel two-wavelength mid-infrared laser-absorption diagnostic method for simultaneous measurements of vapor-phase fuel mole fractions and liquid fuel film thicknesses. Mignot et al. [16] proposed a novel technique to measure liquid film thicknesses up to 2 mm under thermodynamic conditions encountered in a containment during severe accident scenario. Schmidt et al. [17] developed an absorption-based sensor for the measurements of dynamic film thicknesses in a range of 150–400 μm with good accuracy. Pan et al. developed two multi-wavelength diode laser absorption sensors to determine the film thicknesses, temperatures, and solute concentrations of static films for aqueous NaCl solutions [18] and urea–water solutions [19], respectively, but at least one of the two desired parameters (the temperature or concentration) must be known. And Pan et al. presented another sensor by combining two diode lasers at 1412 and 1353 nm to measure the film thicknesses on an opaque surface, however, the liquid film temperature should be provided in advance [20]. Yang et al. presented the simultaneous measurements of film thicknesses, vapor-phase and liquid-phase temperatures with the diode-laser absorption spectroscopy (DLAS) technique by combining four wavenumber positions (7082.89/6714.57/7185.59/7390.13 cm^{-1}) [21]. The absorption theory of Beer-Lambert law was utilized to plenty of applications several decays. However, to the best of the author's knowledge, this is the first time to simultaneously measure the liquid film thickness and temperature of pure water by combining only two wavelengths. In addition, the whole evaporation processes of the static liquid films and the flow processes of dynamic films can be tracked with the developed sensor in the work and serious beam steering effects involved in the relevant processes can be eliminated.

In this paper, a sensor based on the DLAS was developed to simultaneously determine liquid water film thicknesses and temperatures by combining two diode lasers at different wavenumber positions, 6718.2 cm^{-1} and 7040.8 cm^{-1} . And the sensor can be potentially applied in the relevant industrial processes. For instance, the investigation of liquid film outside the horizontal tube in the seawater desalination process is helpful to understand its heat and mass transfer mechanisms, and provide reference data for the optimization of relevant devices. As for the sensor, an integrating sphere was employed to avoid the serious beam steering effects and improve the performance of the sensor for dynamic film investigations. A calibration tool with known film thicknesses and temperatures was firstly utilized to verify the measurement accuracies of the sensor. Furthermore, the sensor was applied to investigate the whole evaporation processes of static films on a horizontal quartz glass plate and flow processes of dynamic films in a flow channel at different film temperatures, respectively.

2. Measurement strategies

For the pure water investigated in the work, based on the Beer-Lambert law, the transmittance $\tau(v_i)$ at the wavenumber v_i of the laser beam passing through the liquid water was described as

$$\tau(v_i) = \left(I_t/I_0 \right) = \exp[n \cdot \sigma(v_i, T_i) \cdot d_i] \quad (1)$$

with the transmitted intensities I_t , the incident intensities I_0 , the liquid temperatures T_i , the liquid water absorption cross sections $\sigma(v_i, T_i)$. The optical path d_i is the length of the absorbing medium, i.e., the liquid film thickness. n [mol/cm^3] is the molar concentration of the liquid water,

$$n = \frac{\rho(T_i)}{M} \quad (2)$$

where ρ [g/cm^3] and M [g/mol] are the densities and the molecular mass of the liquid water, respectively. Table 1 listed the density of liquid water ρ in the range 0–100 $^\circ\text{C}$ [22].

Based on Table 1, the relationship between temperature and the density of liquid water can be expressed with a second-order polynomial fit:

$$\rho(T_i) = 0.73694 + 0.00199T_i - 3.73881 \times 10^{-6}T_i^2 \quad (3)$$

Here, the temperature-dependent densities retained three significant digits. Here, it revealed that the transmittance was only dependent on the film thickness and temperature at specific wavenumber position. Therefore, two wavelengths were employed to determine the two unknown parameters.

Due to the hydrogen bonding [23], liquid water exhibits broadband absorption from OH-stretch vibrational bands in the near-infrared region. The high-resolved liquid water absorption spectra measured at different temperatures from 25 to 75 $^\circ\text{C}$ between 5800 and 7800 cm^{-1} were shown in Fig. 1 [24]. The two-line DLAS sensor was developed mainly based on the variation of absorption spectra of liquid water at different temperatures, because the liquid-water absorption spectrum shifts towards shorter wavelengths with increasing temperature. Laser 1 (6718.2 cm^{-1}) and laser 2 (7040.8 cm^{-1}) (marked as vertical lines in Fig. 1) currently available in the lab were employed to develop the two-line sensor for liquid film investigation. Here, the two-line DLAS sensor was developed to achieve simultaneous measurement of liquid film thickness and temperature, while only film thickness can be determined in reference [24]. Changes in the revised manuscript were provided on page 4. The absorption spectra of water vapor near 7040.8 cm^{-1} and 6718.2 cm^{-1} based on the spectroscopic parameters in HITRAN2016 (High Resolution Transmission Molecular Absorption Database 2016) [25] were plotted in Fig. 2. The central wavenumber positions of laser 1 and 2 (marked as green lines in Fig. 2) are 6721.3 cm^{-1} and 7044.0 cm^{-1} , respectively. The full width at half maximum (FWHM) for both laser 1 and laser 2 are 2 cm^{-1} . Since fixed-wavelength absorption spectroscopy was employed here, the laser output wavenumber positions were fixed at 6718.2 cm^{-1} and 7040.8 cm^{-1} by controlling the temperature and current of the two diode lasers, respectively. Meanwhile,

Table 1
The density of liquid water ρ in the range 0–100 $^\circ\text{C}$.

T_i [$^\circ\text{C}$]	ρ [g/cm^3]
0	0.99984
10	0.99970
20	0.99821
30	0.99565
40	0.99222
50	0.98803
60	0.98320
70	0.97778
80	0.97182
90	0.96535
100	0.95840

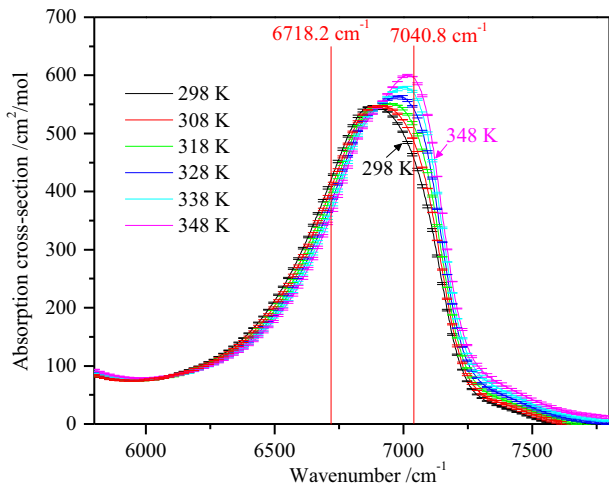


Fig. 1. Absorption spectra of liquid water in the range 5500–8000 cm^{-1} for temperatures between 298 and 348 K.

the line strengths of water vapor at 6718.2 cm^{-1} and 7040.8 cm^{-1} were $3.271\text{e}-10 \text{ cm}^{-2}/\text{atm}$ and $2.134\text{e}-9 \text{ cm}^{-2}/\text{atm}$, respectively. Therefore, the influence of water vapor absorption can be then neglected here.

Since the liquid water absorption cross sections $\sigma(v_i, T_i)$ depends on the specific wavenumber and temperature of liquid water, the $\sigma(v_i, T_i)$ and their linear fit (solid lines) at two wavenumber positions were shown in Fig. 3a, which can be expressed as.

$$\sigma(v_i, T_i) = a_i + b_i T_i \quad i = 1, 2 \quad (4)$$

where a_i and b_i are the respective fitting coefficients as shown in Table 2. It was found that the coefficients of determination R^2 for the linear fit of $\sigma(v_i, T_i)$ with T_i at 6718.2 cm^{-1} and 7040.8 cm^{-1} were 0.9950 and 0.9996, respectively. It showed a significant linear relationship between the absorption cross sections and temperatures.

After combining Eqs. (1)–(4), the transmittance τ was a function of T_i and d_i .

The ratio of the logarithm of the transmissions at two wavenumber positions can be formed as

$$R = \frac{\ln(\tau(v_1))}{\ln(\tau(v_2))} = \frac{\ln(I_{t1}/I_{o1})}{\ln(I_{t2}/I_{o2})} \quad (5)$$

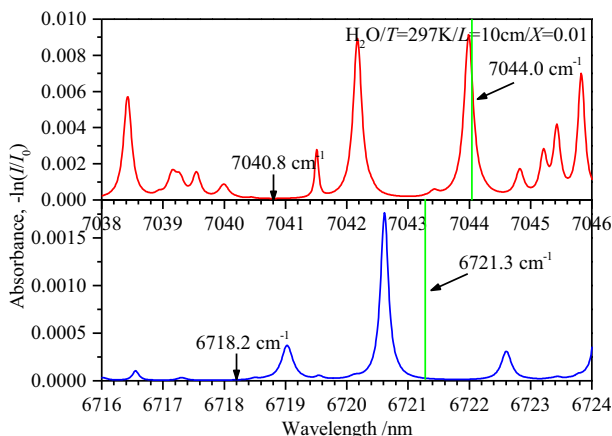


Fig. 2. Absorption spectra of water vapor near 7040.8 cm^{-1} and 6718.2 cm^{-1} .

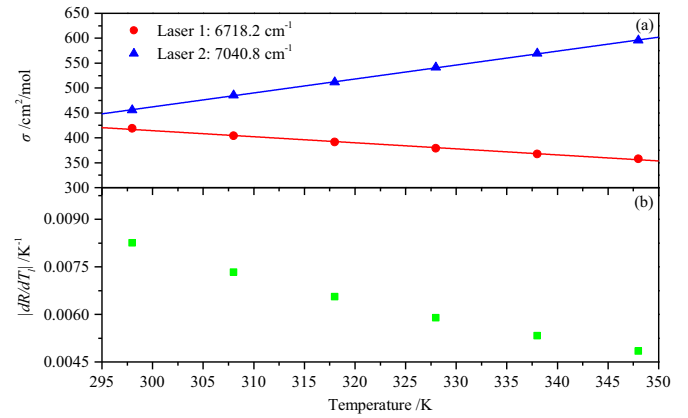


Fig. 3. (a) The liquid water absorption cross sections as a function of temperature at two chosen wavenumber positions (6718.2 cm^{-1} and 7040.8 cm^{-1}). (b) The sensitivity $|dR/dT_i|$ for the combination of laser 1 and laser 2 (green squares).

$$\frac{dR}{dT_i} = \frac{d\sigma_2/dT_i \cdot \sigma_1 - d\sigma_1/dT_i \cdot \sigma_2}{\sigma_2^2} \quad (6)$$

The sensitivity of the measurement with respect to the temperature was related to the absolute value of dR/dT_i , and the sensitivity for the combination of laser 1 and laser 2 was plotted in Fig. 3b. It revealed that with the film temperature increasing from 298 K to 348 K, the $|dR/dT_i|$ decreased by 1.7 times, therefore, the combination of two lasers were good enough here. In addition, it should be noted that the films thicker than 2.0 mm cannot be measured with the combination. The measurement accuracy would be influenced by the non-absorption losses, which were mainly caused by the refraction, i.e., non-flat interface and impurities in water. When the film was not perfectly flat, the optical path was not perpendicular to the mediums interface, an offset should be considered for film thickness measurement. It was found that when the surface of the liquid film was inclined by 45° with respect to the substrate (quartz glass plate), the measured film thickness was 1.07 times as thick as the actual value. And deionized water was employed to avoid the influence from the impurities in water. Table 3 listed the optical refractivities of air calculated with formulas provided by Rueger [26] at different conditions (temperature: 25 °C/35 °C/45 °C and relative humidity: 0%/10%/20%/30%), it revealed that the refractive indices almost kept constant. Therefore, the influence of non-uniformity vapor on the light refraction was slight, the optical path bending problem was then not considered in the work.

Thicker films can be measured by selecting other laser wavelengths with lower absorption cross sections.

The water film temperature T_i can be calculated by inserting Eq. (4) into Eq. (5) for the respective wavenumber positions:

$$T_i = \frac{a_1 - a_2 R}{b_2 R - b_1} \quad (7)$$

When T_i was obtained, the temperature-dependent water absorption cross section $\sigma(v_i, T_i)$ can be determined. However, the direct determination of water absorption cross section was not

Table 2

The fitting parameters of the liquid water absorption cross sections at two wavenumber positions.

Laser	Wavenumber (cm^{-1})	a_i	b_i	R^2
1	6718.2	779.21	-1.22	0.9950
2	7040.8	-377.42	2.80	0.9996

Table 3
Refractivities of the air at different temperature and humidity.

Temperature	Relative humidity	Laser 1	Laser 2
		6718.2 cm ⁻¹	7040.8 cm ⁻¹
		Refractivity (ppm)	Refractivity (ppm)
25 °C	0%	265.532	265.733
	10%	265.412	265.614
	20%	265.293	265.494
	30%	265.173	265.374
35 °C	0%	256.915	257.110
	10%	256.709	256.904
	20%	256.504	256.699
	30%	256.298	256.493
45 °C	0%	248.840	249.029
	10%	246.500	248.689
	20%	248.161	248.349
	30%	247.821	248.010

necessary in the work. By inserting Eq. (7) into Eq. (5), the liquid film thickness d_l can be calculated:

$$d_l = \frac{\ln(\tau(v_1))}{-(a_1 + b_1 T_l) \cdot \frac{\rho(T_l)}{M}} \quad (8)$$

3. Experimental setup and results

3.1. Developed sensor

The developed two-line DLAS sensor was shown in Fig. 4. The laser controller (Thorlabs, PRO8000) was employed to control the temperatures and currents of the two distributed-feedback (DFB) diode lasers (NEL) at constant values to ensure that the output laser wavenumber positions were 6718.2 cm⁻¹ and 7040.8 cm⁻¹, respectively. The two DFB diode lasers were combined by a wavelength division multiplexer (Laser 2000), led through a collimator (Thorlabs, F280APC-C), and then transmitted through the liquid film. The laser beam was perpendicular to the horizontal substrate (quartz glass plate). The diameter of the laser beam at the liquid film was ~1 mm, and it ensured a good spatial resolution of the developed sensor. An integrating sphere (Thorlabs, IS200) was positioned into the transmitted beam path. The inner wall of the integrating sphere was coated with PTFE-based high reflective bulk material with a reflectivity higher than 98% in the near-infrared region. The light from the integrating sphere was received by a

convex lens (Edmund) and focused into a multimode collection fiber (Thorlabs, BFL37-400). Since the inlet of the integrating sphere was 12.5 mm, the laser beams after transmitting through the liquid film can be consistently received by the integrating sphere, therefore, even serious beam steering effects can be avoided. After that, the light was collimated using an aspheric lens (Edmund, diameter: 25 mm, focus length: 25 mm), and then pitched onto a diffraction grating (Edmund, 600 grooves/nm). The two individual wavelengths were diffracted at different angles and then focused onto InGaAs detectors (Thorlabs, PDA10CS-ES). Data acquisition (sampling rate 1 kHz) and post-processing were performed in a LabVIEW environment (National Instruments).

3.2. Validation with a calibration tool

A calibration tool [24] was utilized to verify the measurement accuracies of the two-line DLAS sensor. Deionized water was employed for this and subsequent investigations to avoid the influence from the impurities in water. The known liquid film thickness can be achieved by adjusting the translation stage to change the distance between two horizontal quartz glass plates in the calibration tool, and the distance can be determined by a gauge. The liquid film temperature can be controlled by a heating equipment, and the temperature can be measured by a thermocouple. Fig. 5 showed the results from three repeated measurements when the known liquid film temperatures in the calibration tool were 308 K, 315 K, and 323 K, and the known liquid film thicknesses in the calibration tool were 200, 400, 600, 800 and 1000 μm, respectively. Moreover, the measurements were conducted from thicker film to thinner one (1000 μm down to 200 μm). The liquid temperatures (dashed lines) obtained by the thermocouple slightly decreased with the decreasing film thicknesses, showing a similar trend with the film temperatures (solid symbols) obtained by the DLAS, because the liquid film transferred heat to the upper plate in the calibration tool which was not heated. In addition, in the three repeated experiments, the largest average standard deviation of the measured liquid film thicknesses was 1.6 μm for the measurement at 315 K. And when the known liquid film thickness was 1000 μm, the largest standard deviation of the measured liquid film thicknesses was 3.6 μm. Meanwhile, the largest average standard deviation of the measured liquid film temperatures was 1.1 K for the measurement at 308 K. And when the known liquid film thickness was 400 μm, the largest standard deviation of the measured liquid film temperatures was 1.5 K. It revealed that the measured film thicknesses/temperatures and the corresponding known

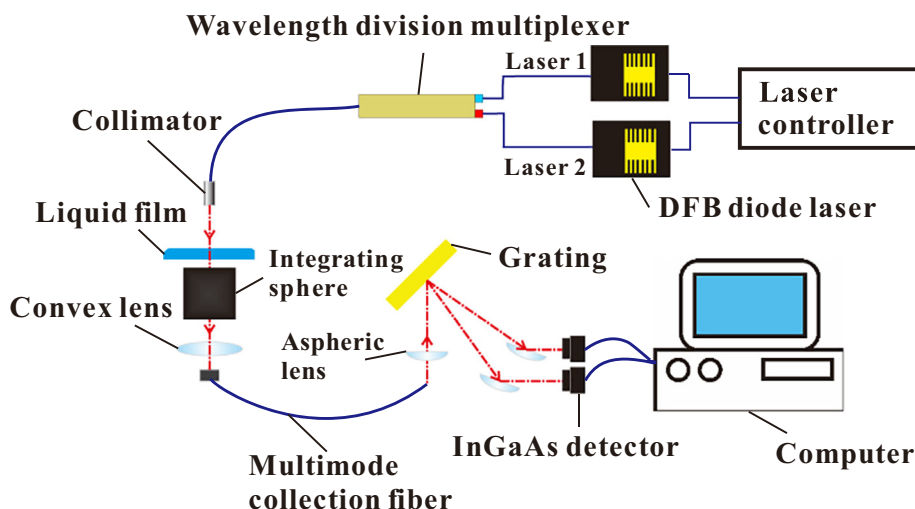


Fig. 4. Schematic drawing of the two-line DLAS sensor.

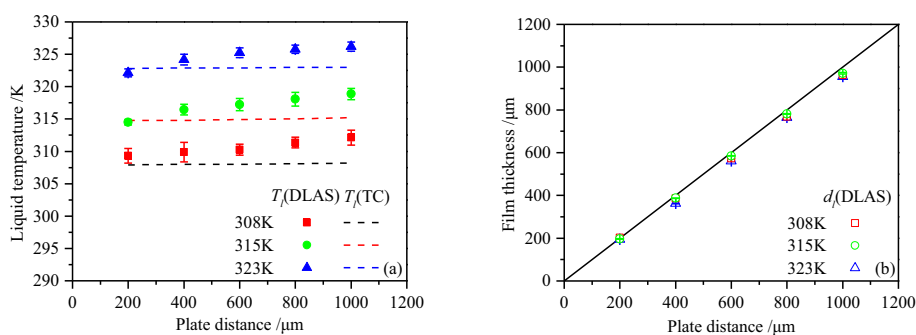


Fig. 5. The measured T_l (a) (filled symbols by DLAS and dashed lines by TC) and d_l (b) (open symbols) as a function of plate distance at three different temperatures (308/315/323 K).

parameters were in good agreements, and the averaged deviations between them were 4.58% and 1.34%, respectively, which was as high as the sensors presented in [20,21,23]. However, the serious beam steering effects cannot be avoided by employing those sensors in the previous researches.

3.3. Application for evaporation process of liquid film

The two-line DLAS sensor was applied to investigate evaporation processes of liquid films with initial film thicknesses $\sim 1500 \mu\text{m}$ on a horizontal quartz glass plate at different temperatures. At the same time, the imaging method and thermocouple were employed to obtain the film thicknesses and temperatures for comparisons with the DLAS, respectively. The experiment setup was shown in Fig. 6. The DLAS sensor was similar to Section 3.1. For the imaging method, a high-power LED as a radiation source and a camera (IMI TECH) with a telecentric lens (XF-MT 0.8×110) were employed. The focal plane of the camera was set at the edge of the quartz glass plate to capture the plate clearly. The images captured by camera were with full resolution (2448×2048 pixels, $3.45 \mu\text{m}$ pixel size) at a frame rate of 12.5 Hz and then post-processed by the computer. The images of up to 256 gray levels were converted into black and white. Threshold was chosen to distinguish the edge of the film based on Otsu's method [27], and the film thickness was then determined. All the processes were automatically achieved by a self-compiled MATLAB program. The diameter of the K-type thermocouple was 0.1 mm. In order not to affect on the shape of the liquid film, the thermocouple was placed 30 mm away from the measured point location of the DLAS. A heat gun (outlet temperatures T_0 were controlled at 340/360/390 K) was used to heat the bottom of the horizontal quartz glass plate. To avoid overloading the figures, the average data in every 30 s were plotted in this section.

Fig. 7 showed the time-dependent intensities of laser 1 and laser 2 in liquid presence (transmitted intensities: I_{t1} : black squares, I_{t2} : red circles) during the film evaporation process at T_0 340 K and without liquid film (incident intensities: I_{01} : green triangles, I_{02} : cyan diamonds) at room temperature. It revealed that the transmitted intensities increased continuously during the evaporation

process, and based on Eqs. (5), (7)–(8), the film thicknesses and temperatures can be determined. It was found that if the noise effects were considered, the measurement accuracies of film thickness and temperature were $1.8 \mu\text{m}$ and 0.2 K , respectively. It indicated that the influence was not obvious, therefore, lock-in amplifier was not employed here.

The variations of film thicknesses (blue triangles: DLAS, cyan squares: imaging method) and temperatures (red circles: DLAS, green diamonds: thermocouple (TC)) as a function of time during the evaporations of the measured liquid films were shown in Fig. 8. In the initial periods of the evaporation processes (0–600/0–540/0–480 s at the three temperatures, respectively), with a low evaporation rates (0.29/0.3/0.41 $\mu\text{m/s}$), the liquid film temperatures increased from room temperature to around 313.4/316.1/325.2 K, respectively. In the middle periods of the evaporation processes (600–3600/540–3600/480–2250 s), the evaporation rates slightly increased (0.34/0.40/0.57 $\mu\text{m/s}$); the liquid film temperatures approximately reached plateaus with average temperatures around 317.9 K, 320.2 K and 327.1 K, respectively. It was observed that there were some fluctuations of the liquid film thickness and temperature due to the shrinkage of the liquid film. The shrinkage was the phenomenon that the surface area of the liquid film reduced due to the influence of surface tension. Since the liquid film contracted and gathered towards its center (i.e. measured point of DLAS method) in the evaporation process, the liquid film thicknesses raised sharply. Moreover, because of the inhomogeneous temperature distribution near the DLAS laser point, the rearrangement of the liquid film caused by shrinkage led to the fluctuations of the temperatures. In addition, the average film temperatures obtained by the thermocouple were 312.1 K, 314.8 K and 323.1 K, respectively. The average deviation of the film temperature obtained by the DLAS and thermocouple was 5.1 K. It could be attributed to the different locations of measured points of these two methods. In the last periods of the evaporation processes (3600–5340/3600–4740/2250–3030 s), due to the liquid film shrunk sharply, the temperatures fluctuated seriously, and the evaporation rates reached the maximum (0.39/0.55/0.74 $\mu\text{m/s}$). In summary, the average evaporation rates of the liquid film obtained by the DLAS method at the

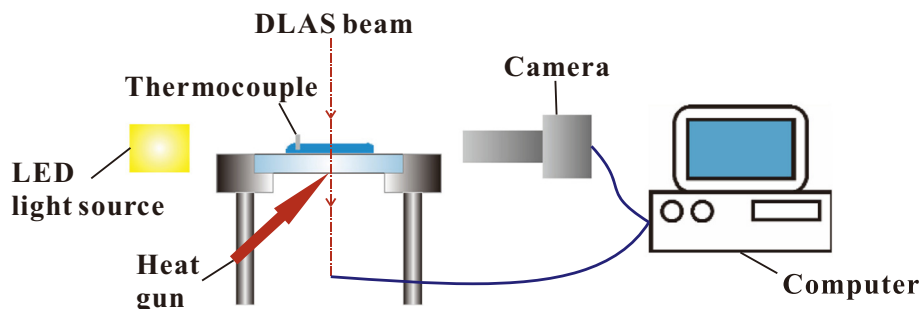


Fig. 6. Experimental setup of the liquid film measurement during the film evaporation process.

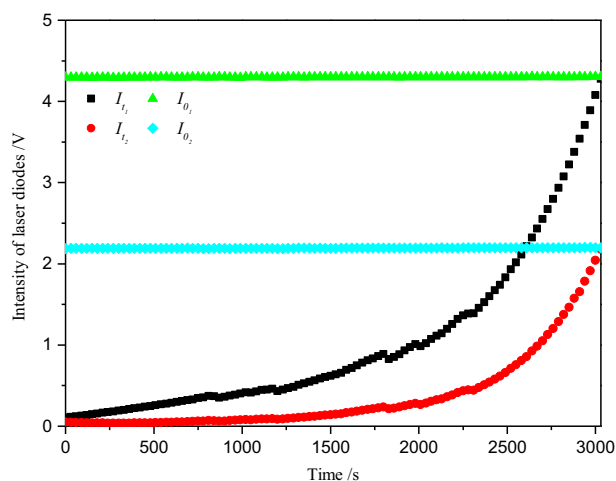


Fig. 7. Time-dependent intensities of laser 1 and laser 2 in liquid film presence (transmitted intensities: I_{t1} ; black squares, I_{t2} ; red circles) during the film evaporation process at T_0 340 K and without liquid film (incident intensities: I_{01} ; green triangles, I_{02} ; cyan diamonds) at room temperature.

three temperatures were 0.34/0.41/0.57 $\mu\text{m/s}$, respectively, and the evaporation rates increased with the increasing film temperatures.

Fig. 9 showed shadowgraph images at four chosen specific instants (960/2280/3000/3600 s) during film evaporation at T_0 340 K, a white horizontal line indicated the interface between the quartz glass plate and the liquid film, and a gray dot in instant 1 marked the point where diode laser beam transmitted through the liquid film. The initial diameter of the liquid film was ~ 10 cm, and the diameter decreased gradually at the end of its evaporation process. Since the width of area taken by the camera was only 1.0551 cm, which was much smaller than the film diameter, the edge shape of water film could not be observed in Fig. 9. At the end of the evaporation process (i.e. after the liquid film decreases to 300 μm), the liquid film was not located in the region of the depth-of-field of the camera, and the film thickness cannot be obtained. The average deviation of liquid film thickness measured by DLAS and imaging method was 105.8 μm . Therefore, the limited depth of field could affect the measurement range and accuracy of the imaging method.

3.4. Application for dynamic liquid film

The two-line DLAS sensor was further applied to obtain the variations of the film thicknesses and temperatures of dynamic liquid films in a flow channel at different temperatures, as the experimental setup shown in Fig. 10. The sensor setup was the same as described in Section 3.1. The channel length and width were 250 mm and 20 mm, respectively, and the channel inclination angle was 5° . The flow channel was made from polymethyl methacrylate (PMMA). The inlet of the flow channel was connected to the peristaltic pump (flow rate 60 ml/min) by plastic tube (0.5 cm diameter). In addition, only peristaltic pump was available in the lab, and further experiments can be performed by utilizing syringe pump in the future work. In order to form liquid films in the entire flow channel, a convex block was arranged 30 mm away from the inlet, while the measured point of the DLAS method was 120 mm away from the inlet. And a plate was glued at the outlet of the channel to provide a stable flow. Here, the integrating sphere was employed to eliminate serious beam steering effects even occurred in turbulent flow. In addition, if the film tends to reshape in droplets, the transmitted light beam will strongly deviate from the original light path, the measurement accuracy of the sensor will be affected. The diameter of incident light beam can be increased to eliminate the specific influence by

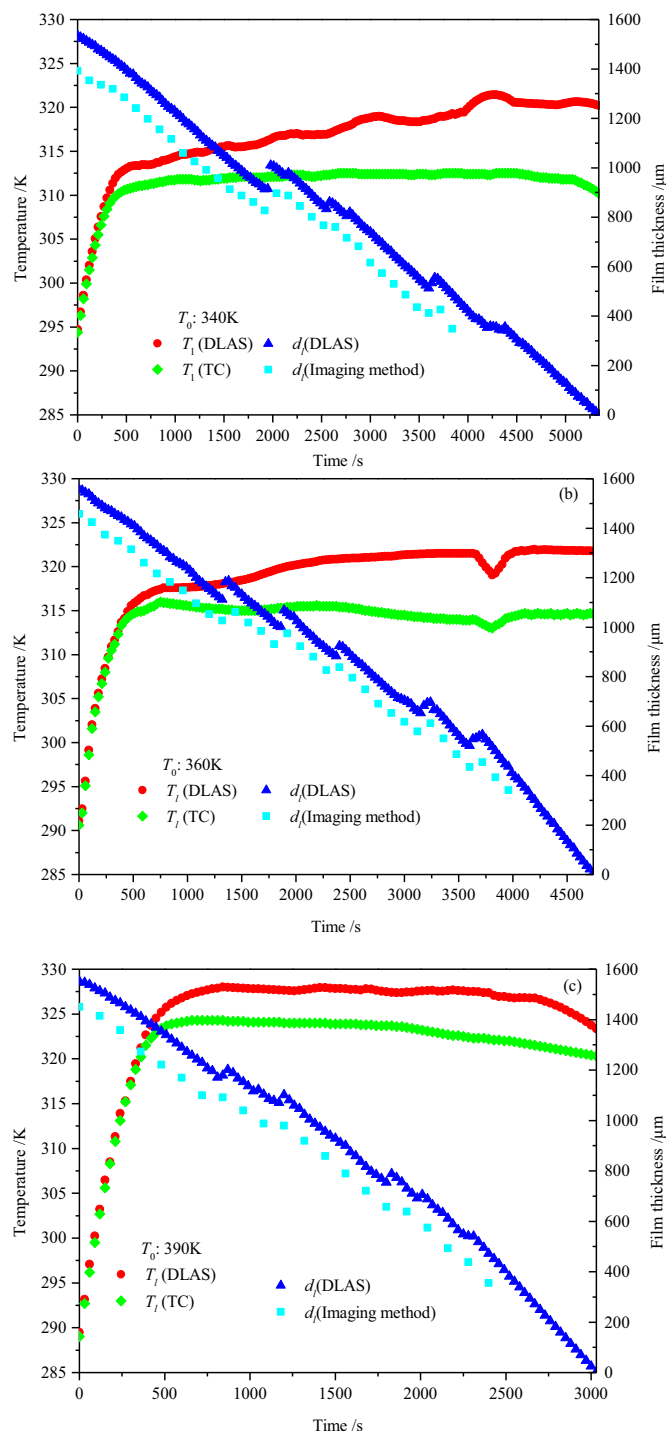


Fig. 8. Time-resolved measurements of the film thicknesses (blue triangles) and film temperatures (red circles) by the DLAS, film thicknesses by the imaging method (cyan squares), and film temperatures by the thermocouple (green diamonds) during the film evaporation processes.

adding optics to improve the performance of the sensor. A thermostat with a certain amount of distilled water was located below the outlet of the flow channel. The temperatures of the water films (308/315/323 K) can be controlled by changing the temperatures of the thermostat. The outlet of the thermostat was connected to the inlet of the peristaltic pump to form a circulating flow. The thermocouple was not employed to compare with the DLAS results here and it can be installed downstream the DLAS sensor in the future work.

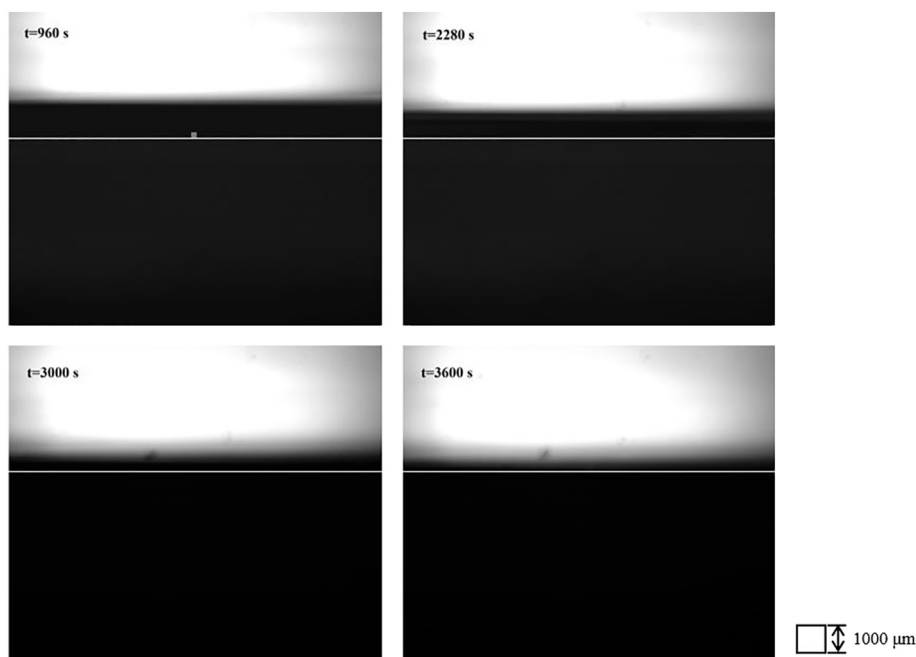


Fig. 9. Shadowgraph images at four specific instants in time of film evaporation at T_0 340 K (t indicated the times of taking images).

Fig. 11 showed the variations of the film thicknesses (blue line) and temperatures (red line) as a function of time in the flow channel obtained by the DLAS at three different temperatures of the water films (308 K, 315 K, and 323 K). It was observed that the trends of the liquid film thickness were “sinusoidal” distributed, which was attributed to the fact that a section of the pump tube between the two rollers in the head of the pump will form “pillow shape” fluid, thus the pump produced a “sinusoidal shape” flow. The average film thicknesses measured by the DLAS at three temperatures were 624.9, 628.6 and 625.7 μm , respectively. In the period of 1 s, there were 11 times fluctuations of the liquid film thicknesses and the average variations of the liquid film thicknesses

were 62.7, 66.3 and 71.2 μm , respectively. And the corresponding maximum film thicknesses were 79.8, 74.9 and 85.9 μm , while the corresponding minimum film thicknesses were -78.6 , -81.0 and -91.9 μm , respectively. The average flow liquid film temperatures were 306.9 K, 313.4 K and 321.2 K, respectively, and the temperature differences between the data obtained by the DLAS and thermostat were 1.1 K, 1.6 K and 1.8 K, respectively. It might be related to the heat losses during the flow of distilled water from the outlet of the thermostat to the inlet of the flow channel. The liquid film temperatures almost stayed constant in the period of 1 s at three temperatures, since the decreases of the film temperatures caused by the heat losses were not obvious in such a short period.

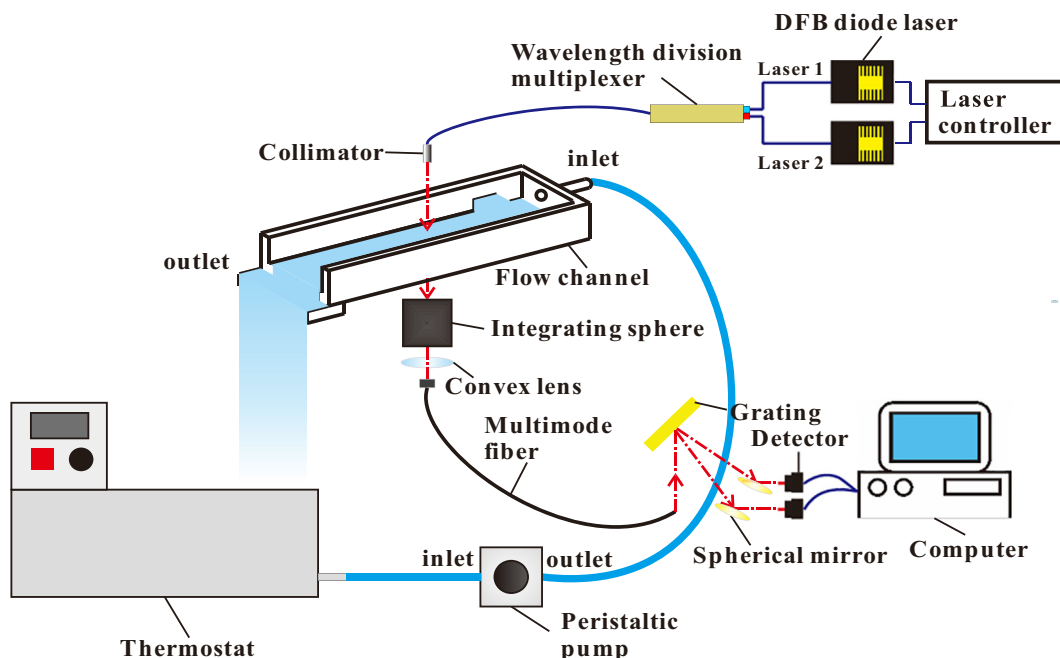


Fig. 10. Experimental setup of the liquid film measurement in a flow channel.

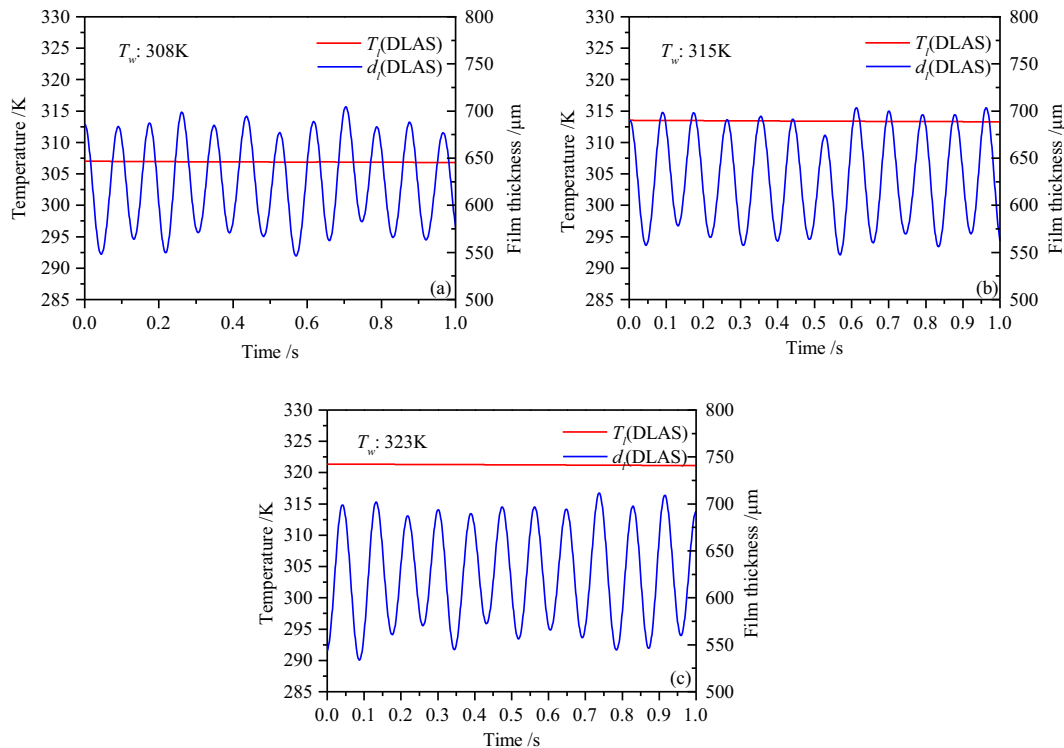


Fig. 11. Variations of the film thicknesses (blue line) and film temperatures (red line) of the flow water films in a flow channel as a function of time at 308 K (a), 315 K (b), and 323 K (c).

4. Conclusions

In the present work, a measurement sensor based on DLAS was developed to simultaneously determine liquid film thicknesses and temperatures by combining two diode lasers with different wave-numbers, 6718.2 cm^{-1} and 7040.8 cm^{-1} . For the validation experiments in a calibration tool, it revealed that the averaged deviations between the measured film thicknesses/temperatures and the corresponding known parameters were 4.58% and 1.34%, respectively. In addition, the sensor was applied to investigate static liquid film evaporation processes at different temperatures. It showed that the average evaporation rates of the liquid film at the heat gun outlet temperatures 340/360/390 K were 0.34, 0.41 and 0.57 $\mu\text{m/s}$, respectively, and the evaporation rates of the liquid films increased with the increasing film temperatures. Furthermore, the sensor was applied to determine the variations of liquid film thicknesses and temperatures in a flow channel. It revealed that the film temperatures remained almost constant during passage of low-amplitude surface waves at the film temperatures 308/315/323 K. The sensor showed a good performance on dynamic film investigations. The temperature control and insulation were not considered in the experimental setup here. We will improve the temperature stability in the future work by employing temperature control and insulation equipment.

Acknowledgments

This work was supported by National Natural Science Foundation of China (NSFC) (Grant No. 51676130, 51776129, U1810129), State Key Laboratory of Applied Optics Open Fund (SKLAO-201909).

References

- [1] X.B. Bu, W.B. Ma, H.S. Li, Heat and mass transfer of ammonia-water in falling film evaporator, *Frontiers in Energy* 5 (4) (2011) 358–366.

- [2] Z.A. Kaklar, M.R. Ansari, Numerical analysis of the internal flow and the mixing chamber length effects on the liquid film thickness exiting from the effervescent atomizer, *J. Therm. Anal. Calorim.* (2018) 1–10.
- [3] M. Mumekata, J. Nishiyama, A. Noguchi, et al., Drying of flowing liquid film on rotating disk, *J. Therm. Sci.* 19 (3) (2010) 234–238.
- [4] A.I. Petrukhin, A.D. Solodukhin, S.P. Fisenko, Simulation of cooling of water droplet and film flows in large natural wet cooling towers, *J. Eng. Phys. Thermophys.* 74 (1) (2001) 62–68.
- [5] S. Grout, J. Blaisot, K. Pajot, et al., Experimental investigation on the injection of an urea–water solution in hot air stream for the SCR application: evaporation and spray/wall interaction, *Fuel* 106 (2013) 166–177.
- [6] W. Ambrosini, N. Forgiione, F. Oriolo, Statistical characteristics of a water film falling down a flat plate at different inclinations and temperatures, *Int. J. Multiphase Flow* (9) (2002) 1521–1540.
- [7] W.W. Wang, C.G. Li, X.J. Wang, et al., A study on measurement of thickness of thin liquid film on metal surfaces, *Dongfang Turbine* 01 (2010) 21–25.
- [8] W.P. Yan, H.T. Li, X.M. Ye, et al., A study of the transient non-contact measurement of vertical free-falling liquid-film thickness, *Journal of Engineering for Thermal Energy & Power* 04 (2007) 380–384.
- [9] Charogiannis A, Markides C N. Spatiotemporally resolved heat transfer measurements in falling liquid-films by simultaneous application of planar laser-induced fluorescence (PLIF), particle tracking velocimetry (PTV) and infrared (IR) thermography. *Exp. Thermal Fluid Sci.* 2018.
- [10] D. Greszik, H. Yang, T. Dreier, et al., Measurement of water film thickness by laser-induced fluorescence and Raman imaging, *Applied Physics B* (1) (2011) 123–132.
- [11] A.V. Cherdantsev, D.B. Hann, B.N. Hewakandamby, et al., Study of the impacts of droplets deposited from the gas core onto a gas-sheared liquid film, *Int. J. Multiphase Flow* 88 (2017) 69–86.
- [12] C.H. Hidrovo, D.P. Hart, Emission reabsorption laser induced fluorescence (ERLIF) film thickness measurement, *Meas. Sci. Technol.* 12 (4) (2001) 467–477.
- [13] M. Leng, S. Chang, H. Wu, Experimental investigation of shear-driven water film flows on horizontal metal plate, *Exp. Thermal Fluid Sci.* 94 (2018) 134–147.
- [14] W. Clark, *The Interfacial Characteristics of Falling Film Reactors*, University of Nottingham, 2001, pp. 108–127.
- [15] J.M. Porter, J.B. Jeffries, R.K. Hanson, Mid-infrared laser-absorption diagnostic for vapor-phase fuel mole fraction and liquid fuel film thickness, *Applied Physics B* 102 (2) (2011) 345–355.
- [16] G. Mignot, J. Dupont, S. Paranjape, et al., Measurement of liquid films thickness in a condensing and re-evaporating environment using attenuation of near infrared light, *Nucl. Eng. Des.* 336 (2018) 64–73.
- [17] A. Schmidt, B. Kuhnreich, H. Kittel, et al., Laser based measurement of water film thickness for the application in exhaust after-treatment processes, *Int. J.*

- Heat Fluid Flow 71 (2018) 288–294.
- [18] R. Pan, J.B. Jeffries, T. Dreier, et al., Measurements of liquid film thickness, concentration and temperature of aqueous NaCl solution by NIR absorption spectroscopy, *Applied Physics B* 120 (3) (2015) 397–406.
- [19] R. Pan, J.B. Jeffries, T. Dreier, et al., Measurements of liquid film thickness, concentration, and temperature of aqueous urea solution by NIR absorption spectroscopy, *Applied Physics B* 122 (1) (2016) 4.
- [20] R. Pan, C. Brocksieper, J.B. Jeffries, et al., Diode laser-based standoff absorption measurement of water film thickness in retro-reflection, *Applied Physics B* 122 (2016) 249.
- [21] H. Yang, D. Greszik, I. Wlokas, et al., Tunable diode laser absorption sensor for the simultaneous measurement of water film thickness, liquid- and vapor-phase temperature, *Applied Physics B* 104 (2011) 21–27.
- [22] David R. Lide (Ed.), *CRC Handbook of Chemistry and Physics*, Internet Version 2005, CRC Press, Boca Raton, FL, 2005, p. 986. <http://www.hbcpnetbase.com>.
- [23] G.M. Hale, M.R. Query, Optical constants of water in the 200-nm to 200- μm wavelength region, *Appl. Opt.* (3) (1973) 555–563.
- [24] H. Yang, D. Greszik, T. Dreier, et al., Simultaneous measurement of liquid water film thickness and vapor temperature using near-infrared tunable diode laser spectroscopy, *Applied Physics B* 99 (3) (2010) 385–390.
- [25] I.E. Gordon, L.S. Rothman, C. Hill, et al., The HITRAN2016 molecular spectroscopic database, *J. Quant. Spectrosc. Radiat. Transf.* 203 (2017) 3–69.
- [26] J.M. Rueger, *Refractive Indices of Light, Infrared and Radio Waves in the Atmosphere*, School of Surveying and Spatial Information Systems, University of New South Wales, Sydney, Australia, 2002.
- [27] N. Otsu, A threshold selection method from gray-level histograms, *IEEE Transactions on Systems, Man, and Cybernetics* 9 (1) (1979) 62–66.